

1 **On the variation in the ionospheric response to**  
2 **geomagnetic storms with time of onset**

K. R. Greer,<sup>1</sup> T. Immel,<sup>1</sup> A. Ridley,<sup>2</sup>

3 Simulations reproduce observed dependence of ionospheric response to UT of storm onset.

4 Changes in upper atmospheric neutral winds or composition cannot account for the ionospheric  
5 effect at low latitudes

6 The implicated driver is the coupling of storm time F-regions winds and Earth's asymmetric  
7 magnetic topology

---

Corresponding author: K. R. Greer, Space Science Lab, University of California- Berkeley, 7  
Gauss Way, Berkeley, CA 94720, USA. (greerk@ssl.berkeley.edu)

<sup>1</sup>Space Sciences Lab, University of  
California- Berkeley, Berkeley, CA, USA.

<sup>2</sup>Department of Aerospace Engineering,  
University of Michigan, Ann Arbor, MI,  
USA.

**This is the author manuscript accepted for publication and has undergone full peer review but has not been through the copyediting, typesetting, pagination and proofreading process, which may lead to differences between this version and the Version of Record. Please cite this article**

as doi:10.1002/2016JA023457 March 17, 2017, 2:11am

D R A F T

**Abstract.**

Recent observations from *Immel and Mannucci* [2013] have indicated that geomagnetic storms cause larger enhancements in the ionospheric plasma density and total electron content (TEC) in the American sector than anywhere else on the planet. This suggests that the presence of a UT storm onset effect that is important for correctly understanding the impact, longitudinal structure and timing of geomagnetic storms. Using the Global Ionosphere-Thermosphere Model (GITM) we conduct a modeling experiment of the August 2011 geomagnetic storm by modifying the storm arrival time (UT) in Earth's daily rotation and examining the subsequent system response. We find that the simulations reflect the recent studies indicating the strongest enhancements of TEC are in the American and Pacific longitude sectors of storms with onsets between 1600 UT and 2400 UT. The underlying mechanisms of the strong TEC increases during storm times in these longitude sectors are also examined. Some of the resulting TEC structure may be explained by changes in the  $[O]/[N_2]$  ratio (especially in the high-latitudes), but it is unable to explain all of the variability in the equatorial regions. Storm time neutral winds and vertical ion motions coupled to Earth's asymmetrical geomagnetic topology appear to be driving the longitude sector variability due to UT storm onset times.

## 1. Introduction

28 Interest in understanding the detailed behavior of Earth's ionosphere has increased  
29 as reliance on satellite communication and navigation has grown. These technologies are  
30 susceptible to unpredicted variability in ionospheric plasma density and intensified density  
31 gradients. The availability of these technologies is therefore influenced by ionospheric  
32 'weather,' and the prediction of ionospheric conditions continues to be challenging because  
33 of limitations in the observations of key parameters and numerical models [*Komjathy et al.*,  
34 2005]. Progress in modeling the key influences and drivers of this complex and dynamic  
35 region continues to be made. However, with the continued deployment of ground-based  
36 line of sight Total Electron Content (TEC) receivers [*Jakowski et al.*, 2002a; *Kintner and*  
37 *Ledvina*, 2005; *Valladares and Chau*, 2012] and space-based occultation receivers [*Jakowski*  
38 *et al.*, 2002b; *Lei et al.*, 2007; *Hajj and Romans*, 1998], there is a growing accurate record  
39 of ionospheric plasma. Though spatial and temporal gaps do exist in these records, we  
40 are able to observe the global morphology of ionospheric storms in increasing detail. The  
41 technologies and systems that are adversely affected by elevated density and sharp density  
42 gradients also serve to provide measurements of the changing plasma parameters. These  
43 kinds of observations have lead to several breakthroughs in our knowledge of the Earth-  
44 Sun system behavior during magnetic storms.

45 The positive ionospheric storm has long been observed in daytime plasma densities,  
46 particularly in the afternoon sector [*Mendillo et al.*, 1970; *Burns et al.*, 1995a]. Related  
47 inner-magnetospheric signatures of ionospheric plasma enhancements were first described  
48 by *Grebowsky et al.* [1978] [see also *Carpenter et al.* [1992]] and seen in imaging of the

49 plasmasphere by the NASA Magnetopause-to-Aurora Global Exploration (IMAGE) mis-  
50 sion [Sandel *et al.*, 2001; Burch, 2003]. Through multi-point measurements of plasma  
51 density, it has been shown that plasma density enhancements in the daytime are highly  
52 structured and reflect, in part, the development of inner-magnetospheric electric fields  
53 that are only manifested during these disturbed periods [Foster and Rich, 1998; Huang  
54 *et al.*, 2005]. The structure and evolution of ionospheric density enhancements, particu-  
55 larly those observed early in geomagnetic storms, reflect both causes and signatures that  
56 extend throughout the geospace system.

57 Numerical and observational studies of the variability of ionospheric features in the mid-  
58 and low-latitudes have been conducted over the years, however there are limited studies  
59 focused exclusively on longitudinal variability due to the universal time (UT) onset time  
60 in the low latitudes. Explorations of the longitude sector differences of equatorial spread  
61 F have been conducted by several groups [Aarons, 1991; Fejer *et al.*, 1999; Abdu *et al.*,  
62 2005; Oladipo *et al.*, 2014] and several studies have found an impact of longitudinal effects  
63 on the equatorial electrojet (EEJ) [England *et al.*, 2006; Klimenko and Klimenko, 2015;  
64 Yizengaw *et al.*, 2014; Phani Chandrasekhar *et al.*, 2014]. It has also been recognized  
65 that the neutral atmosphere plays a critical role through nonmigrating tidal influences  
66 [Immel *et al.*, 2006; Forbes *et al.*, 2008; Maute *et al.*, 2015] and longitudinally dependent  
67 thermospheric winds [Fuller-Rowell *et al.*, 1994; Sojka *et al.*, 2012] in the distribution  
68 of plasma. And while there are numerous studies examining enhancements of TEC [Ho  
69 *et al.*, 1996; Kelley *et al.*, 2004; Mendillo, 2006], a proxy measurement for plasma density,  
70 during geomagnetic storms, far fewer studies have been concerned with the variability of  
71 that TEC distribution based on the UT time (longitudinally dependent) onset of storms at

72 low- and mid-latitudes [*Immel and Mannucci*, 2013; *Coster et al.*, 2007]. *Mendillo* [2006]  
73 conducted a statistical epoch analysis of TEC storms observed by Air Force Cambridge  
74 Research Laboratories (AFCRL) locations in the Northern Hemisphere organized by local  
75 time (LT), but the actual UT onset time was not kept as a factor and the lowest latitude  
76 site was Kennedy Space Flight Center. An idealized modeling study conducted by *Sojka*  
77 *et al.* [2012] found TEC enhancements had preferential longitudinal sectors in the mid-  
78 latitudes based on onset-times, but limitations of the model meant that low-latitude and  
79 equatorial processes were explicitly excluded from their analysis. Through a statistical  
80 examination of ionospheric conditions during all geomagnetic storms observed during the  
81 1998-2007 epoch, *Immel and Mannucci* [2013] found that for storms with onsets between  
82 1800 UT and 2200 UT, large storm time increases in daytime ionospheric plasma content  
83 exists in the American sector and is stronger there than in any other sector. However, the  
84 methodology of this study was limited by being obliged to draw conclusions from sparse  
85 data (TEC observations are especially scarce over oceans) and comparisons of phenomeno-  
86 logically disparate geomagnetic storms. Additionally, their examination of observational  
87 TEC maps is not able isolate and implicate the driving mechanisms responsible for this  
88 UT onset longitudinal variability; coupled global numerical simulations would be ideal  
89 for examining this through numerical experiments of storms that onset at different times,  
90 but are otherwise identical storms. It has yet to be shown that available coupled mod-  
91 els have been able to replicate the zonal effect observed by *Immel and Mannucci* [2013],  
92 or reproduce a UT variation in storm densities at the middle and low latitudes as ob-  
93 served in the JPL GNSS-TEC (Jet Propulsion Laboratory's Global Navigation Satellite  
94 System) data assimilated from quiet and storm-time measurements. The use of sophis-

95 ticated coupled numerical simulations allows us to investigate whether the observed UT  
96 onset longitudinal sector variability is a physically driven phenomenon, or potentially due  
97 to observational geometry or sparseness of data over particular geographic regions. Re-  
98 producing this phenomenon and investigating its drivers comprise the motivations of this  
99 work.

100 This study investigates a case in August 2011 where a solar wind disturbance impacted  
101 geospace and drove an isolated but strong geomagnetic storm response. We use the specific  
102 inputs of this storm to investigate the importance of the UT storm onset and longitudinal  
103 sector response. Here we show that the coupled Global-Ionosphere-Thermosphere Model  
104 (GITM), using time shifted magnetospheric inputs developed using BATS-R-US (Block  
105 Adaptive Tree SolarWind-Roe Upwind Scheme), displays a remarkable low and middle  
106 latitude asymmetry in responses to the storm. Further, it indicates for the first time that  
107 chemical, dynamical, and electrodynamic drivers all have the potential to play a key role  
108 in supporting the larger TEC increases observed in the South American sector during this  
109 August 2011 storm. We specifically compare the wind dynamo, magnetospheric potentials,  
110 and thermospheric composition to the storm enhanced density to identify the key drivers  
111 of the plasma density increases for different storm onset UT.

## 2. Model

112 A coupled model of the ionosphere and thermosphere that simultaneously captures the  
113 physics of both the neutral and plasma environments is required for this investigation.  
114 This is because the variable composition and dynamics of the upper atmosphere during  
115 geomagnetic storms are critical for modifying the ionosphere, and impacting TEC vari-  
116 ability. By repeatedly modeling the same single observed storm, we remove the inherent

117 variability by that is present in the comparisons of different historical storms having differ-  
118 ent UT onset times and perhaps wildly different solar wind conditions, seasons, durations  
119 and strengths (such as was done by *Immel and Mannucci* [2013]). Further, using a coupled  
120 model may allow the probing of individual driving forces that influence the longitudinal  
121 sector variability due to UT onset.

122 The model used in this study is the Global-Ionosphere-Thermosphere Model (GITM) de-  
123 veloped at the University of Michigan by *Ridley et al.* [2006]. GITM is a three-dimensional,  
124 spherical coordinate model that non-hydrostatically solves the continuity, momentum and  
125 energy equations of the thermosphere and ionosphere using realistic source terms. Ion  
126 flow velocities are assumed to be steady state and solved from the momentum equations.  
127 Physical drivers of the model include auroral particle precipitation, solar extreme ultravi-  
128 olet (EUV) flux, and tides which are determined from the empirical Mass-Spectrometer-  
129 Incoherent-Scatter (MSIS-86) model for the neutral atmosphere below 100 km [*Hedin,*  
130 1987]. The vertical coordinate is altitude while the International Geomagnetic Reference  
131 Field (IGRF) is used for the magnetic topology. The equatorial electrodynamicss are self-  
132 consistently solved [*Richmond, 1995*]. The high latitude electric fields are supplied by  
133 the Space Weather Modeling Framework (SWMF) at the Goddard Space Flight Center's  
134 Community Coordinated Modeling Center (CCMC). The CCMC archives these inputs  
135 and they may be accessed by the public on their website or by request.

136 For the experimental runs, the geographical grid was specified as  $5^\circ$  longitude x  $2^\circ$   
137 latitude with an altitude range of 100 km to 600 km. A value of 1750 was used for  
138 the eddy diffusion coefficient [*Pawlowski and Ridley, 2009*]. The model was allowed 48  
139 simulation hours to spin-up using Weimer high-latitude electric fields [*Weimer, 1996*], then,

140 15 hours before the onset of storm conditions (and throughout the duration of the storm),  
141 the model was driven by the more realistic high-latitude electric field drivers provided  
142 by the Space Weather Modeling Framework's BATS-R-US model (please visit SWMF at  
143 <http://ccmc.gsfc.nasa.gov/> for more information)[*Tóth et al., 2005*].

144 A limitation of GITM may sometimes be seen in unusual night-time modeled plasma val-  
145 ues that do not accurately reflect observed plasma densities, particularly at mid-latitudes.  
146 Factors in the current version of GITM that may be contributing to this are that vertical  
147 advection of ions are computed using  $\ln(\rho)$  as the quantity in the solver for the vertical ad-  
148 vection scheme (to linearize the exponentially decreasing mass density with altitude) and  
149 a model simplification introduced to the continuity equation for the ions which assumes  
150 that the contribution from the divergence of the wind field is negligible. Further inves-  
151 tigation of this model during quiet-time conditions is discussed in *Vichare et al. [2012]*.  
152 Given that this study is focused on differences between model runs under identical inputs  
153 shifted in UT, for our conclusions these limitations are of little consequence.

### 3. Methods

154 To investigate UT-dependent responses of the ionosphere, we used the moderately strong  
155 geomagnetic storm that was observed in August 2011 during the International Union of  
156 Radio Science (URSI) World Day Campaign. The sun during solar cycle 24 has been un-  
157 usually quiet, but 2011 was part of the two-peaked solar maximum when there were more  
158 frequent flares and Coronal Mass Ejections (CMEs). The Dst (nT) and Interplanetary  
159 Magnetic Field (IMF) for 04:00 UT on 5 August through 12:00 UT on 7 August 2011 are  
160 shown in Figure 1. The intensity of the IMF was measured by the Advanced Composition  
161 Explorer (ACE), while the Dst is provided by the Kyoto World Data Center [*Sugiura,*



162 1964]. Two CMEs were propelled from the Sun, merged, and arrived at Earth, causing an  
163 abrupt increase in the dynamic pressure, strong oscillations in all components of the IMF  
164 [Huang *et al.*, 2014] and a brief rise in Dst followed by a precipitous drop. The vertical red  
165 line in Figure 1 indicates the onset time of the storm at 19:06 UT on 5 August 2011. The  
166 Dst index reached a minimum value of -115 nT at 04:00 UT on 6 August 2011 while the  
167 Kp index reached 7+, indicative of a strong geomagnetic storm. An extended recovery  
168 followed.

169 Although GITM has been extensively validated in literature [Ridley *et al.*, 2006; Deng  
170 *et al.*, 2008; Pawlowski *et al.*, 2008; Zhu and Ridley, 2016; Zhu *et al.*, 2016], Figure  
171 2 shows a comparison of TEC obtained from GNSS (GPS) and modeled by GITM  
172 for the geomagnetic storm shown in Figure 1. GPS TEC data was obtained from  
173 <ftp://spdf.gsfc.nasa.gov/pub/data/gps/> and is 2-hourly maps of TEC as derived by the  
174 International GNSS Service (IGS)[Kouba, 2009]. Figure 2 shows the progression of the  
175 TEC in local time (LT) in the equatorial and mid-latitudes at 107 W (North America and  
176 Eastern Pacific sector) in TECu ( $10^{16} e^-/m^2$ ). The white vertical line at local 12-noon  
177 indicates the onset of the geomagnetic storm (5 August 2011 19:06 UT). In general, GITM  
178 captures the timing of the evolving structure well, but tends to underestimate the after-  
179 noon mid-latitude TEC. Given the modeling simplifications made by GITM it appears  
180 that at low latitudes the vertical gradient in the ion velocity in the vertical direction may  
181 be significant and strongly affect the plasma density structure with height, causing the ion  
182 densities to be lofted too high in the ionosphere late in the day, reducing the loss rates,  
183 and causing the densities at night to be too large. Nonetheless, the plasma densities and

184 associated TEC results from GITM during the daytime are reliable and appropriate for  
185 use in studies of *relative* change in TEC such as this particular study.

186 Using GITM, we modeled this storm with the observed timing, where at 19:06 UT the  
187 sector around  $107^\circ$  W was at solar local noon. For subsequent runs the arrival time of the  
188 driving solar wind inputs were shifted in time to examine how the ionosphere responded  
189 to different UT storm onsets, for the same solar wind conditions. The storm onset times  
190 were shifted by -12, -9, -6, -3, +3, +6, +9, and +12 hours, which correspond to sunward  
191 arrival sectors (1200 LT) of  $72^\circ$ E,  $27^\circ$ E,  $17^\circ$ W,  $62^\circ$ W,  $152^\circ$ W,  $162^\circ$ E,  $117^\circ$ E and  $72^\circ$ E,  
192 respectively.

193 To obtain a picture of how ionospheric conditions vary with UT timing of the storm,  
194 we make use of global maps of Total Electron Content (TEC). These are calculated from  
195 column plasma densities produced by GITM. To evaluate changes in the ionosphere pro-  
196 duced by storms, the change between quiet solar wind conditions to storm conditions can  
197 be compared at any longitude sector or local time. The mean quiet-time TEC as modeled  
198 by GITM is shown in Figure 3 for the longitude sectors of  $0^\circ$ E,  $90^\circ$ E,  $0^\circ$ W and  $90^\circ$ W.  
199 This mean quiet-time was determined by using the 15 hours prior to storm onset for all  
200 nine model runs (since these runs were shifted in time by up to 12 hours, it allowed for  
201 the build up of 24 hours of quiet ionosphere). The quiet TEC was calculated for each  
202 longitude-latitude grid point, every 900 seconds (15 minutes). In each case, the Equatorial  
203 Ionospheric Anomaly (EIA) is prominent at low latitudes from approximately 1000 LT  
204 to 1800 LT at all longitudes. Maximum quiet-condition TEC values generally reached  
205 approximately 35 TECu in the Southern crest of the EIA. Even during quiet ionospheric  
206 conditions, Figure 3 clearly shows that different longitude sectors have different local time

207 responses in terms of magnitude, timing and structure of plasma in the ionosphere. It  
208 is critical to take into account this natural quiet-time variability when evaluating the  
209 ionosphere's response to the storm conditions.

#### 4. TEC Plasma Results

210 The difference between active and quiet conditions for each of the experimental storm  
211 onset times is shown in Figure 4. Each panel is for a constant longitude focusing on  
212 the afternoon and evening hours; the colors indicate the absolute difference,  $TEC_{Storm} -$   
213  $TEC_{Quiet}$ , in latitude and local time. The longitude displayed corresponds to the longitude  
214 of 1200 LT (the sunward sector) at the time of the onset of the storm, and a stereographic  
215 map of the Earth is provided for geographic reference. These experiments span  $\pm 12$   
216 hours from the observed onset at 1900 UT. Additionally, these results are also presented  
217 as percent change in TEC for additional insight in Figure 5.

218 All the experiments share some general features. At low latitudes there is deepening of  
219 the depletion of plasma in the trough of the EIA, especially pronounced after 1800 LT. On  
220 either side of this depletion, there is an augmentation of TEC. This is consistent with the  
221 observations from *Immel and Mannucci* [2013] of historical storm TEC with Dst indices  
222 of  $< -100$  nT where there is an enhancement of the fountain effect driven by penetration  
223 of magnetospheric electric fields into the low-latitudes [*Mannucci et al.*, 2005].

224 However, Figure 4 also exhibits TEC structures that are slowly varying between the  
225 different storm onset experiments. In the evening hours, the sectors between 62W and  
226 162E (the Americas and central Pacific) display an intense but narrow tongue of con-  
227 centrated TEC in the Southern hemisphere just below the equatorial trough, an increase  
228 of approximately 20 TECu or percent change of nearly 90%. Hemispheric asymmetry is

likely due to the season and configuration of the geomagnetic field. Large positive differences extend to higher latitudes between noon and 1400 LT in the sectors between 152W and 117E, over the Pacific ocean and Eastern Asia, of 10-12 TECU or a percent change of 40-60%. The Western Pacific sector around 162E is the only sector that experiences a period (around 1715 LT) where the trough feature in the EIA is diminished.

It is evident from these results that the American and Pacific sectors in the southern hemisphere experience the strongest TEC enhancements, in intensity, duration, and latitudinal extent for these storm conditions. These enhancements develop approximately 2 hours after the onset of the storm and extend past sunset. These results indicate that the density and prominence of daytime plasma structures at mid- and low-latitude do, in fact, depend on the UT of storm onset (sunward longitude sector) and that GITM is capable of reproducing this effect.

## 5. Drivers of Variability Impacted by UT Onset

By interrogating the model outputs for each experiment, we can examine drivers of the variability seen in the model by changing the UT (sunward longitude sector) of the storm onset. We consider several drivers including variations in the  $[O]/[N_2]$  ratio, neutral winds, and the geomagnetic topology.

### 5.1. O/N<sub>2</sub> Ratio

Changes in TEC plasma populations, such as those in Figure 4 and Figure 5, may be attributed to changes in the sources or sinks of plasma populations. The  $[O]/[N_2]$  ratio is a strong indicator of the population source of plasma in the ionosphere and is a relevant consideration when examining changes in TEC [Burns *et al.*, 1995b]. It is also indicative

249 of the controlling influence of the neutral atmosphere on the ionosphere. Figure 6 shows  
250 the percent change in the  $[O]/[N_2]$  ratio (storm conditions compared to quiet conditions)  
251 for selected experimental runs for constant longitude sectors. In the high latitudes of the  
252 Southern Hemisphere, there is a substantial reduction of the  $[O]/[N_2]$  ratio of up to 30%  
253 near  $60^\circ$  at 1600 LT for storm onsets between 0400 UT and 1000 UT. The reduced  $[O]/[N_2]$   
254 ratio likely contributes strongly to the depletion of TEC in this particular geographic area.  
255 While the equatorial region indicates a 10-15% decline in  $[O]/[N_2]$  ratio (between storm  
256 onsets starting at 1000 and 1600 UT) compared to quiet conditions, this is not triggered  
257 by the onset of storm conditions and cannot be identified as the main driver of the changes  
258 in the plasma populations. Other drivers must be considered.

## 5.2. Neutral Winds

259 Given that changes in the loss and production of plasma by way of the  $[O]/[N_2]$  ratio  
260 do not adequately account for the modeled changes in TEC, an explanation is sought in  
261 effects of stormtime neutral winds at ionosphere altitudes. Neutral winds drag the  
262 embedded plasma along with it. When a component of the neutral wind is parallel to the  
263 magnetic field, it can push plasma along the field lines [*Bramley and Young, 1968; Burrell*  
264 *et al., 2012, 2013*]. Enhanced equatorward winds can therefore potentially affect plasma  
265 densities by lifting the F-layer and reducing loss through recombination [*Rishbeth et al.,*  
266 *1987*]. While the plasma resists moving across magnetic field lines, other factors may  
267 induce vertical drift. As the electric field is modified by disturbance winds, storm-driven  
268 electric fields may penetrate to lower latitudes due to an active ring current, phenomena  
269 such as Sub-Auroral Polarization Stream (SAPS) and disturbance dynamo driven currents  
270 prompt potentials that can cause the plasma to drift upward as well [*Blanc and Rich-*

271 *mond*, 1980; *Heelis*, 2004]. Therefore, both zonal and meridional winds are considered as  
272 potential sources of TEC disturbance, and the potential UT dependence of these drivers  
273 is investigated.

274 Wind vectors for the experimental model runs at 307 km are shown in Figure 7. Each  
275 panel is for a constant longitude; the contoured colors behind the vectors indicate the  
276 change in the zonal wind from quiet conditions in latitude and local time.

277 At local noon and storm onset, F-region winds are generally westward at low latitudes  
278 in all experiments. However, onsets between 0400 and 1000 UT show moderate winds  
279 that are more Eastward in the mid- and high-latitude southern hemisphere at noon. Two  
280 hours later, the wind vectors at 1400 LT show strikingly different behaviors between the  
281 different experiments, where both the magnitudes and directions of the winds are variable  
282 between longitudes. There is a strong band of Eastward winds near 45°S which persists  
283 throughout in all experiments, except those with onset times of 1600 UT and 1900 UT.  
284 In sectors expected to be near the auroral oval in the Southern Hemisphere, there is a  
285 pronounced acceleration of winds.

286 Zonal wind differences between quiet and storm time are on the order of 100-200 m/s  
287 throughout low- and mid- latitudes, growing as the storm continues in the 8 hours following  
288 onset shown in Figure 7. The zonal winds in the equatorial region become more eastward  
289 or anti-sunward, through the rest of the afternoon compared to quiet conditions. Though  
290 the simulation predicts large changes in F-region winds, variations in the zonal winds  
291 are not consistent with being the main driver of the TEC changes shown earlier. The  
292 meridional effects are much smaller and not of the magnitude necessary to produce a

293 major uplift of the F-layer that might influence the balance of F-layer production and  
294 loss.

295 While there is significant variation between longitudes in the neutral winds, the im-  
296 pact of these winds on the plasma distribution is intimately coupled to the geomagnetic  
297 topology as the charged particles are constrained by the magnetic field lines. Given that  
298 Earth's geomagnetic field is tilted, any ExB drift will therefore have a vertical component  
299 [*Deng and Ridley, 2006*]. The influence of the neutral wind needs to be considered in  
300 combination with Earth's geomagnetic field in order to understand the 3D motion of the  
301 plasma which may be inducing the TEC structures seen in this experiment.

### 5.3. Geomagnetic Topology

302 Plasmas embedded within the neutral winds interact with and are constrained by  
303 Earth's non-uniform geomagnetic topology. Previous studies have found that as a dis-  
304 turbance from a solar flare propagates through the nightside and back to the dayside, the  
305 magnetic field may have a large impact on the response of the ionosphere [*Zhu and Ri-*  
306 *dley, 2014*]. The International Geomagnetic Reference Field (IGRF) [*Finlay et al., 2010*]  
307 intensity [ $\text{nT} \cdot 10$ ] for August 2011 is shown in Figure 8 as solid black contours. Earth  
308 has an irregular quasi-dipole field that is both tilted and offset from the planet's axis of  
309 rotation. Large anomalies exist in this field: at the equator, the poles, and particularly  
310 around South America [*Knecht and Shuman, 1985; Malin and Isakara, 1976*]. Overlaid  
311 on the IGRF intensity is vertical plasma velocity at 1600 LT (4 hours after the onset of  
312 the storm) for the modeling experiments shown in Figure 7. This local time was chosen  
313 because it is the local time with the greatest changes between modeling experiments as  
314 seen in TEC (Figure 2).

315 Vertical plasma motion shows extensive variability in latitude, local time (not shown),  
316 and between modeling experiments. During quiet conditions there is an equatorial band  
317 of rising plasma, while off the equator, plasma is descending as expected along magnetic  
318 field lines. Stronger descent is seen over the South Atlantic Anomaly. However, during  
319 storm conditions, plasma there is less descent at nearly all latitudes with the exception  
320 of longitudes around South of Africa. In the final panel, the difference between storm  
321 and quiet ion vertical velocities is shown. However, this vertical ion motion varies greatly  
322 by longitude sector. There is a zonal band of increased vertical ion motion in Northern  
323 Hemisphere at mid- and low-latitudes that peaks in over North America. Critically, there  
324 is one longitude sector that stands out in particular: the Americas and Eastern Pacific  
325 longitude sector of the storm that onsets at 1900 UT. This sector experiences more vertical  
326 motion than any other at nearly all latitudes. As the plasma is lofted higher in altitude  
327 it experiences reduced loss (by recombination), which leads to higher TEC. Southern  
328 hemispheric preferences may be due not only to seasonal differences, but also because  
329 of the greater separation between the geographic and geomagnetic poles [*Fuller-Rowell*  
330 *et al.*, 1988]. Given the limited correspondence between the TEC variation and other  
331 parameters shown, we conclude that this property is the critical and determining factor  
332 in the development of increased low and middle latitude plasma in this sector during  
333 storms.

## 6. Conclusions

334 We have performed a series of modeling experiments with GITM in which the August  
335 2011 geomagnetic storm solar wind inputs were shifted in universal time, such that dif-  
336 ferent longitude sectors were sunward when the the storm commenced. GITM shows



337 a remarkable UT dependent effect of ionospheric conditions at low latitudes following  
338 storm onset. Specifically, the 1900 UT sector at onset produces the largest enhancement  
339 in ionospheric TEC at low to middle latitudes, particularly in the Southern Hemisphere.  
340 Further, this result matched the relatively sparse observations of UT variation in storm-  
341 time ionospheric effects observed in global TEC maps by *Immel and Mannucci* [2013],  
342 which showed a similar relationship between the UT onset time of a given storm and  
343 the structure and evolution of TEC in the middle latitude ionosphere, favoring (again)  
344 the Southern Hemisphere. In a broader sense, during this modeled geomagnetic storm  
345 period, larger TEC were produced by GITM over the American and Eastern Pacific lon-  
346 gitude sectors of the afternoon Southern Hemisphere, which corresponds to storms that  
347 onset between 1600 and 2400 UT. For communications and navigation technologies that  
348 have critical dependencies on ionospheric conditions, these results imply larger impacts  
349 on their availability for storms that onset at these between these hours.

350 Possible driving mechanisms for this longitudinal asymmetry were found to include  
351 changes in  $[O]/[N_2]$  ratios, changes in the neutral winds and asymmetries in Earth's  
352 geomagnetic topology. In the high-latitude southern hemisphere a 30% reduction in the  
353  $[O]/[N_2]$  ratio is likely responsible for strong depletions in TEC. However, changes in  
354  $[O]/[N_2]$  ratios could not account for the changes and structure of TEC in low- and mid-  
355 latitudes. The neutral horizontal winds at at F-region altitudes showed marked variability  
356 between model experiments, but the motion of plasma is also closely coupled to Earth's  
357 magnetic field. It is likely that the explanation for the longitudinal and UT dependence  
358 of the ionosphere is that it is driven by changes in neutral winds and interaction with

359 Earth's tilted and distorted magnetic field, which reaches its most southern latitudes and  
360 greatest gradient in declination in the South American sector.

361 **Acknowledgments.** This work was supported by NSF Grants AGS1103333 and  
362 AGS1019065. GITM was driven from time-shifted inputs archived by the Space Weather  
363 Modeling Framework at the Goddard Space Flight Center's Community Coordinated  
364 Modeling Center and can be accessed at [http://ccmc.gsfc.nasa.gov/ungrouped/GM\\_IM/GM\\_main.php](http://ccmc.gsfc.nasa.gov/ungrouped/GM_IM/GM_main.php)  
365 and searching for the string 'Greer'. The link to the ACE data depository is  
366 <http://www.srl.caltech.edu/ACE/ASC/level2/index.html>, and the data are also available  
367 at <http://cdaweb.gsfc.nasa.gov/>. The National Oceanic and Atmospheric Administration  
368 (NOAA) provided hemispheric power index data (<http://www.swpc.noaa.gov/ftpmenu/lists/hpi.html>)  
369 to drive the high-latitude auroral precipitation. The results from the GITM simulations  
370 are publicly available. Because of the considerable amount of data (several gigabytes),  
371 the results can only be obtained on request from the main author. The GITM model was  
372 developed by the University of Michigan (contact: Aaron Ridley, [ridley@umich.edu](mailto:ridley@umich.edu)). We  
373 would like to acknowledge high-performance computing support from Yellowstone pro-  
374 vided by NCAR's Computational and Information Systems Laboratory, sponsored by the  
375 National Science Foundation.

## References

376 Aarons, J. (1991), The role of the ring current in the generation or inhibition of equatorial  
377 f layer irregularities during magnetic storms, *Radio Science*, *26*(4), 1131–1149, doi:  
378 10.1029/91RS00473.

- 379 Abdu, M., I. Batista, A. Carrasco, and C. Brum (2005), South atlantic magnetic anomaly  
380 ionization: A review and a new focus on electrodynamic effects in the equatorial iono-  
381 sphere, *Journal of Atmospheric and Solar-Terrestrial Physics*, *67*(1718), 1643 – 1657,  
382 doi:<http://dx.doi.org/10.1016/j.jastp.2005.01.014>.
- 383 Blanc, M., and A. D. Richmond (1980), The ionospheric disturbance dynamo, *Journal of*  
384 *Geophysical Research*, *85*, 1669–1688.
- 385 Bramley, E., and M. Young (1968), Winds and electromagnetic drifts in the equato-  
386 rial f2-region, *Journal of Atmospheric and Terrestrial Physics*, *30*(1), 99 – 111, doi:  
387 [http://dx.doi.org/10.1016/0021-9169\(68\)90044-5](http://dx.doi.org/10.1016/0021-9169(68)90044-5).
- 388 Burch, J. (2003), The first two years of image, in *Magnetospheric Imaging The Image*  
389 *Prime Mission*, edited by J. Burch, pp. 1–24, Springer Netherlands.
- 390 Burns, A. G., T. L. Killeen, W. Deng, and G. R. Carignan (1995a), Geomagnetic storm  
391 effects in the low- to middle-latitude upper thermosphere, *Journal of Geophysical Re-*  
392 *search*, *100*, 14,673–14,691.
- 393 Burns, A. G., T. L. Killeen, G. R. Carignan, and R. G. Roble (1995b), Large enhancements  
394 of the o/n<sub>2</sub> ratio in the evening sector of the winter hemisphere during geomagnetic  
395 storms, *Journal of Geophysical Research*, *100*, 14,673–14,691.
- 396 Burrell, A. G., R. A. Heelis, and R. A. Stoneback (2012), Equatorial longitude and local  
397 time variations of topside magnetic field-aligned ion drifts at solar minimum, *Journal*  
398 *of Geophysical Research: Space Physics*, *117*(A4), doi:10.1029/2011JA017264, a04304.
- 399 Burrell, A. G., R. A. Heelis, and A. Ridley (2013), Daytime altitude variations of the  
400 equatorial, topside magnetic field-aligned ion transport at solar minimum, *Journal of*  
401 *Geophysical Research: Space Physics*, *118*(6), 3568–3575, doi:10.1002/jgra.50284.

- 402 Carpenter, D. L., A. J. Smith, B. L. Giles, C. R. Chappell, and P. M. E. Decreau (1992),  
403 A case study of plasma structure in the dusk sector associated with enhanced magne-  
404 topheric convection, *Journal of Geophysical Research*, *97*, 1157–1166.
- 405 Coster, A. J., M. J. Colerico, J. C. Foster, W. Rideout, and F. Rich (2007), Longitude sec-  
406 tor comparisons of storm enhanced density, *Geophysical Research Letters*, *34*, L18105,  
407 doi:10.1029/2007GL030682.
- 408 Deng, Y., and A. Ridley (2006), The role of vertical ion convection in the high-latitude  
409 ionospheric plasma distribution, *Journal of Geophysical Research*, *97*, 1157–1166, doi:  
410 10.1029/2006JA011637.
- 411 Deng, Y., A. D. Richmond, A. J. Ridley, and H.-L. Liu (2008), Assessment of the non-  
412 hydrostatic effect on the upper atmosphere using a general circulation model (gcm),  
413 *Geophysical Research Letters*, *35*(1), doi:10.1029/2007GL032182, L01104.
- 414 England, S. L., S. Maus, T. J. Immel, and S. B. Mende (2006), Longitudinal variation of  
415 the e-region electric fields caused by atmospheric tides, *Geophysical Research Letters*,  
416 *33*(21), doi:10.1029/2006GL027465, L21105.
- 417 Fejer, B. G., L. Scherliess, and E. R. de Paula (1999), Effects of the vertical plasma drift  
418 velocity on the generation and evolution of equatorial spread F, *Journal of Geophysical*  
419 *Research*, *104*, 19,859–19,870, doi:10.1029/1999JA900271.
- 420 Finlay, C. C., S. Maus, C. D. Beggan, T. N. Bondar, A. Chambodut, T. A. Cher-  
421 nova, A. Chulliat, V. P. Golovkov, B. Hamilton, M. Hamoudi, R. Holme, G. Hulot,  
422 W. Kuang, B. Langlais, V. Lesur, F. J. Lowes, H. Lhr, S. Macmillan, M. Manda, S.  
423 McLean, C. Manoj, M. Menvielle, I. Michaelis, N. Olsen, J. Rauberg, M. Rother, T. J.  
424 Sabaka, A. Tangborn, L. Tffner-Clausen, E. Thbault, A. W. P. Thomson, I. Wardinski,

- 425 Z. Wei, and T. I. Zvereva (2010), International geomagnetic reference field: the eleventh  
426 generation, *Geophysical Journal International*, *183*(3), 1216–1230, doi:10.1111/j.1365-  
427 246X.2010.04804.x.
- 428 Forbes, J. M., X. Zhang, S. Palo, J. Russell, C. J. Mertens, and M. Mlynczak (2008),  
429 Tidal variability in the ionospheric dynamo region, *Journal of Geophysical Research*,  
430 *113*, A02310, doi:10.1029/2007JA012737.
- 431 Foster, J. C., and F. J. Rich (1998), Prompt mid-latitude electric field effects during  
432 severe geomagnetic storms, *Journal of Geophysical Research*, *103*, 26,367–26, 372, doi:  
433 10.1029/2007JA012737.
- 434 Fuller-Rowell, T., D. Rees, S. Quegan, R. Moffett, and G. Bailey (1988), Simulations  
435 of the seasonal and universal time variations of the high-latitude thermosphere and  
436 ionosphere using a coupled, three-dimensional, model, in *Ionospheric Modelling*, edited  
437 by J. Korenkov, Pageoph Topical Volumes, pp. 189–217, Birkhäuser Basel.
- 438 Fuller-Rowell, T. J., M. V. Codrescu, R. J. Moffett, and S. Quegan (1994), Response of the  
439 thermosphere and ionosphere to geomagnetic storms, *Journal of Geophysical Research*,  
440 *99*, 3893–3914.
- 441 Grebowsky, J. M., I. Hoffman, and N. C. Maynard (1978), Ionospheric and mag-  
442 netospheric “plasmapauses”, *Planetary and Space Science*, *26*(7), 651 – 660, doi:  
443 [http://dx.doi.org/10.1016/0032-0633\(78\)90098-3](http://dx.doi.org/10.1016/0032-0633(78)90098-3).
- 444 Hajj, G., and L. Romans (1998), Ionospheric electron density profiles obtained with the  
445 global positioning system: Results from the GPS/MET experiment, *Radio Science*,  
446 *33*(1), 175–190, doi:10.1029/97RS03183.

- 447 Hedin, A. E. (1987), MSIS-86 Thermospheric Model, *Journal of Geophysical Research*,  
448 *92*(11), 4649–4662.
- 449 Heelis, R. A. (2004), Electrodynamics in the low and middle latitude ionosphere:  
450 A tutorial, *Journal of Atmospheric and Terrestrial Physics*, *66*, 825–838, doi:  
451 10.1016/j.jastp.2004.01.034.
- 452 Ho, C. M., A. J. Mannucci, U. J. Lindqwister, X. Pi, and B. T. Tsurutani (1996), Global  
453 ionosphere perturbations monitored by the worldwide GPS network, *Geophysical Re-*  
454 *search Letters*, *23*(22), 3219–3222, doi:10.1029/96GL02763.
- 455 Huang, C.-S., J. C. Foster, and M. C. Kelley (2005), Long-duration penetration of the  
456 interplanetary electric field to the low-latitude ionosphere during the main phase of  
457 magnetic storms, *Journal of Geophysical Research: Space Physics*, *110*(A11), doi:  
458 10.1029/2005JA011202, A11309.
- 459 Huang, C. Y., Y.-J. Su, E. K. Sutton, D. R. Weimer, and R. L. Davidson (2014), Energy  
460 coupling during the august 2011 magnetic storm, *Journal of Geophysical Research:*  
461 *Space Physics*, *119*(2), 1219–1232, doi:10.1002/2013JA019297.
- 462 Immel, T. J., and A. J. Mannucci (2013), Ionospheric redistribution during geomag-  
463 netic storms, *Journal of Geophysical Research: Space Physics*, *118*(12), 7928–7939,  
464 doi:10.1002/2013JA018919.
- 465 Immel, T. J., E. Sagawa, S. L. England, S. B. Henderson, M. E. Hagan, S. B. Mende,  
466 H. U. Frey, C. M. Swenson, and L. J. Paxton (2006), Control of equatorial iono-  
467 spheric morphology by atmospheric tides, *Geophysical Research Letters*, *33*, L15108,  
468 doi:10.1029/2006GL026161.

- 469 Jakowski, N., S. Heise, A. Wehrenpennig, S. Schlter, and R. Reimer (2002a),  
470 GPS/GLONASS-based {TEC} measurements as a contributor for space weather fore-  
471 cast, *Journal of Atmospheric and Solar-Terrestrial Physics*, *64*(56), 729 – 735, doi:  
472 [http://dx.doi.org/10.1016/S1364-6826\(02\)00034-2](http://dx.doi.org/10.1016/S1364-6826(02)00034-2).
- 473 Jakowski, N., A. Wehrenpennig, S. Heise, C. Reigber, H. Lhr, L. Grunwaldt, and  
474 T. K. Meehan (2002b), GPS radio occultation measurements of the ionosphere  
475 from CHAMP: Early results, *Geophysical Research Letters*, *29*(10), 951–954, doi:  
476 [10.1029/2001GL014364](https://doi.org/10.1029/2001GL014364).
- 477 Kelley, M. C., M. N. Vlasov, J. C. Foster, and A. J. Coster (2004), A quantitative ex-  
478 planation for the phenomenon known as storm-enhanced density, *Geophysical Research*  
479 *Letters*, *31*, L19809, doi:[10.1029/2004GL020875](https://doi.org/10.1029/2004GL020875).
- 480 Kintner, P. M., and B. M. Ledvina (2005), The ionosphere, radio navigation, and  
481 global navigation satellite systems, *Advances in Space Research*, *35*(5), 788 – 811, doi:  
482 <http://dx.doi.org/10.1016/j.asr.2004.12.076>.
- 483 Klimenko, V., and M. Klimenko (2015), EEJ and EIA variations during modeling sub-  
484 storms with different onset moments, *Advances in Space Research*, *56*(9), 1982 – 1991,  
485 doi:<http://dx.doi.org/10.1016/j.asr.2015.07.041>.
- 486 Knecht, D. J., and B. M. Shuman (1985), The geomagnetic field, in *Handbook of Geo-*  
487 *physics and the Space Environment*, edited by A. S. Jursa, chapter 4, Air Force Geo-  
488 physics Laboratory.
- 489 Komjathy, A., L. Sparks, A. J. Mannucci, and A. Coster (2005), The ionospheric impact  
490 of the October 2003 storm event on wide area augmentation system, *GPS Solutions*,  
491 *9*(1), 41–50, doi:[10.1007/s10291-004-0126-2](https://doi.org/10.1007/s10291-004-0126-2).

- 492 Kouba, J. (2009), A guide to using international GNSS service (IGS) products.
- 493 Lei, J., S. Syndergaard, A. G. Burns, S. C. Solomon, W. Wang, Z. Zeng, R. G. Roble,  
494 Q. Wu, Y.-H. Kuo, J. M. Holt, S.-R. Zhang, D. L. Hysell, F. S. Rodrigues, and C. H.  
495 Lin (2007), Comparison of cosmic ionospheric measurements with ground- based obser-  
496 vations and model predictions: Preliminary results, *Journal of Geophysical Research:*  
497 *Space Physics*, *112*, A07308, doi:10.1029/2006JA012240.
- 498 Malin, S., and A. M. Isakara (1976), Annual variation of the geomagnetic field, *Geophysical*  
499 *Journal of the Royal Astronomical Society*, *47*, 445–457.
- 500 Mannucci, A. J., B. T. Tsurutani, B. A. Iijima, A. Komjathy, A. Saito, W. D. Gonzalez,  
501 F. L. Guarneri, J. U. Kozyra, and R. Skoug (2005), Dayside global ionospheric re-  
502 sponse to the major interplanetary events of October 29-30, 2003 “Halloween Storms”,  
503 *Geophysical Research Letters*, *32*, L12S02, doi:10.1029/2004GL021467.
- 504 Maute, A., M. E. Hagan, V. Yudin, H.-L. Liu, and E. Yizengaw (2015), Causes of the  
505 longitudinal differences in the equatorial vertical  $E \times B$  drift during the 2013 SSW pe-  
506 riod as simulated by the TIME-GCM, *Journal of Geophysical Research: Space Physics*,  
507 *120*(6), 5117–5136, doi:10.1002/2015JA021126.
- 508 Mendillo, M. (2006), Storms in the ionosphere: Patterns and processes for total electron  
509 content, *Reviews of Geophysics*, *44*(4), RG4001, doi:10.1029/2005RG000193.
- 510 Mendillo, M., M. Papagiannis, and J. A. Klobuchar (1970), Ionospheric storms at mid-  
511 latitudes, *Radio Science*, *5*, 895–898, doi:10.1029/RS005i006p00895.
- 512 Oladipo, O. A., J. O. Adeniyi, A. O. Olawepo, and P. H. Doherty (2014), Large-scale  
513 ionospheric irregularities occurrence at Ilorin, Nigeria, *Space Weather*, *12*(5), 300–305,  
514 doi:10.1002/2013SW000991.



- 515 Pawlowski, D. J., and A. J. Ridley (2009), Quantifying the effect of thermospheric pa-  
516 rameterization in a global model, *Journal of Atmospheric and Solar-Terrestrial Physics*,  
517 *71*(1718), 2017–2026, doi:http://dx.doi.org/10.1016/j.jastp.2009.09.007.
- 518 Pawlowski, D. J., A. J. Ridley, I. Kim, and D. S. Bernstein (2008), Global model com-  
519 parison with Millstone Hill during September 2005, *Journal of Geophysical Research:*  
520 *Space Physics*, *113*(A1).
- 521 Phani Chandrasekhar, N., K. Arora, and N. Nagarajan (2014), Characterization of sea-  
522 sonal and longitudinal variability of EEJ in the Indian region, *Journal of Geophysical*  
523 *Research: Space Physics*, *119*(12), 10,242–10,259, doi:10.1002/2014JA020183.
- 524 Richmond, A. D. (1995), Ionospheric electrodynamics using magnetic APEX coordinates,  
525 *Journal of Geomagnetism and Geoelectricity*, *47*(2), 191–212, doi:10.5636/jgg.47.191.
- 526 Ridley, A. J., Y. Deng, and G. Tóth (2006), The Global Ionosphere Thermosphere  
527 Model, *Journal of Atmospheric and Solar-Terrestrial Physics*, *68*, 839–864, doi:  
528 10.1016/j.jastp.2006.01.008.
- 529 Rishbeth, H., T. J. Fuller-Rowell, and D. Rees (1987), Diffusive equilibrium and vertical  
530 motion in the thermosphere during a severe magnetic storm : A computational study,  
531 *Planetary and Space Science*, *35*, 1157–1165, doi:10.1016/0032-0633(87)90022-5.
- 532 Sandel, B. R., R. A. King, W. T. Forrester, D. L. Gallagher, A. L. Broadfoot, and C. C.  
533 Curtis (2001), Initial results from the IMAGE Extreme Ultraviolet imager, *Geophysical*  
534 *Research Letters*, *28*(8), 1439–1442, doi:10.1029/2001GL012885.
- 535 Sojka, J. J., M. David, R. W. Schunk, and R. A. Heelis (2012), A modeling study of  
536 the longitudinal dependence of storm time mid-latitude dayside total electron con-  
537 tent enhancements, *Journal of Geophysical Research: Space Physics*, *117*(A2), doi:

538 10.1029/2011JA017000.

539 Sugiura, M. (1964), Hourly values of equatorial Dst for the IGY, in *Annual International*  
540 *Geophysical Year*, vol. 35, p. 9, Pergamon, New York.

541 Tóth, G., I. V. Sokolov, T. I. Gombosi, D. R. Chesney, C. R. Clauer, D. L. De Zeeuw,  
542 K. C. Hansen, K. J. Kane, W. B. Manchester, R. C. Oehmke, K. G. Powell, A. J.  
543 Ridley, I. I. Roussev, Q. F. Stout, O. Volberg, R. A. Wolf, S. Sazykin, A. Chan, B. Yu,  
544 and J. Kta (2005), Space Weather Modeling Framework: A new tool for the space  
545 science community, *Journal of Geophysical Research: Space Physics*, 110, A12226, doi:  
546 10.1029/2005JA011126.

547 Valladares, C. E., and J. L. Chau (2012), The Low-latitude Ionosphere Sensor network:  
548 Initial results, *Radio Science*, 47(4), doi:10.1029/2011RS004978.

549 Vichare, G., A. Ridley, and E. Yiğit (2012), Quiet-time low latitude ionospheric elec-  
550 trodynamics in the non-hydrostatic Global IonosphereThermosphere Model, *Journal of*  
551 *Atmospheric and Solar-Terrestrial Physics*, 80, 161–172.

552 Weimer, D. R. (1996), A flexible, IMF dependent model of high-latitude electric potentials  
553 having “space weather” applications, *Geophysical Research Letters*, 23, 2549–2552, doi:  
554 10.1029/96GL02255.

555 Yizengaw, E., M. B. Moldwin, E. Zesta, C. M. Biouele, B. Damtie, A. Mebrahtu, B. Rabiou,  
556 C. F. Valladares, and R. Stoneback (2014), The longitudinal variability of equatorial  
557 electrojet and vertical drift velocity in the African and American sectors, *Annales Geo-*  
558 *physicae*, 32(3), 231–238, doi:10.5194/angeo-32-231-2014.

559 Zhu, J., and A. J. Ridley (2014), The effect of background conditions on the ionospheric  
560 response to solar flares, *Journal of Geophysical Research: Space Physics*, 119(6), 5060–

**Figure 1.** August 2011 Storm Dst index and observed IMF properties.

**Figure 2.** August 2011 Storm TEC (in TECu) at 107 W longitude as observed by GPS (upper plot) and GITM (lower plot). TEC is illustrated in local time (LT) and latitude at a constant longitude. The white vertical line at local 12-noon indicates the onset of the geomagnetic storm (5 August 2011 19:06 UT).

**Figure 3.** Quiet TEC as modeled by GITM for constant longitude sectors in local time and latitude.

**Figure 4.** Difference between quiet TEC and storm time TEC for different experimental storm onset times. Each panel is for a constant longitude, the colors indicate the TEC difference in latitude and local time. The longitude depicted corresponds to the longitude of 1200 LT at the time of onset of storm conditions.

**Figure 5.** Same as Figure 4 but for the percent change in TEC between quiet conditions and storm conditions.

5075, doi:10.1002/2014JA019887.

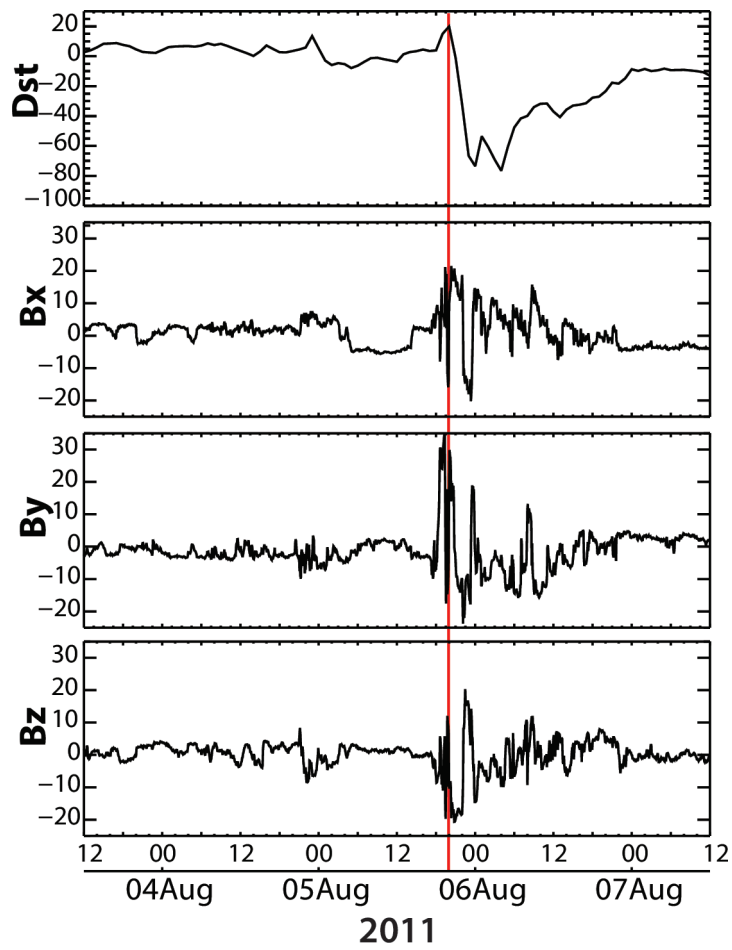
Zhu, J., and A. J. Ridley (2016), Investigating the performance of simplified neutral-ion collisional heating rate in a global IT model, *Journal of Geophysical Research: Space Physics*, 121(1), 578–588, doi:10.1002/2015JA021637.

Zhu, J., A. J. Ridley, and Y. Deng (2016), Simulating electron and ion temperature in a global ionosphere thermosphere model: Validation and modeling an idealized sub-storm, *Journal of Atmospheric and Solar-Terrestrial Physics*, 138139, 243 – 260, doi: <http://dx.doi.org/10.1016/j.jastp.2016.01.005>.

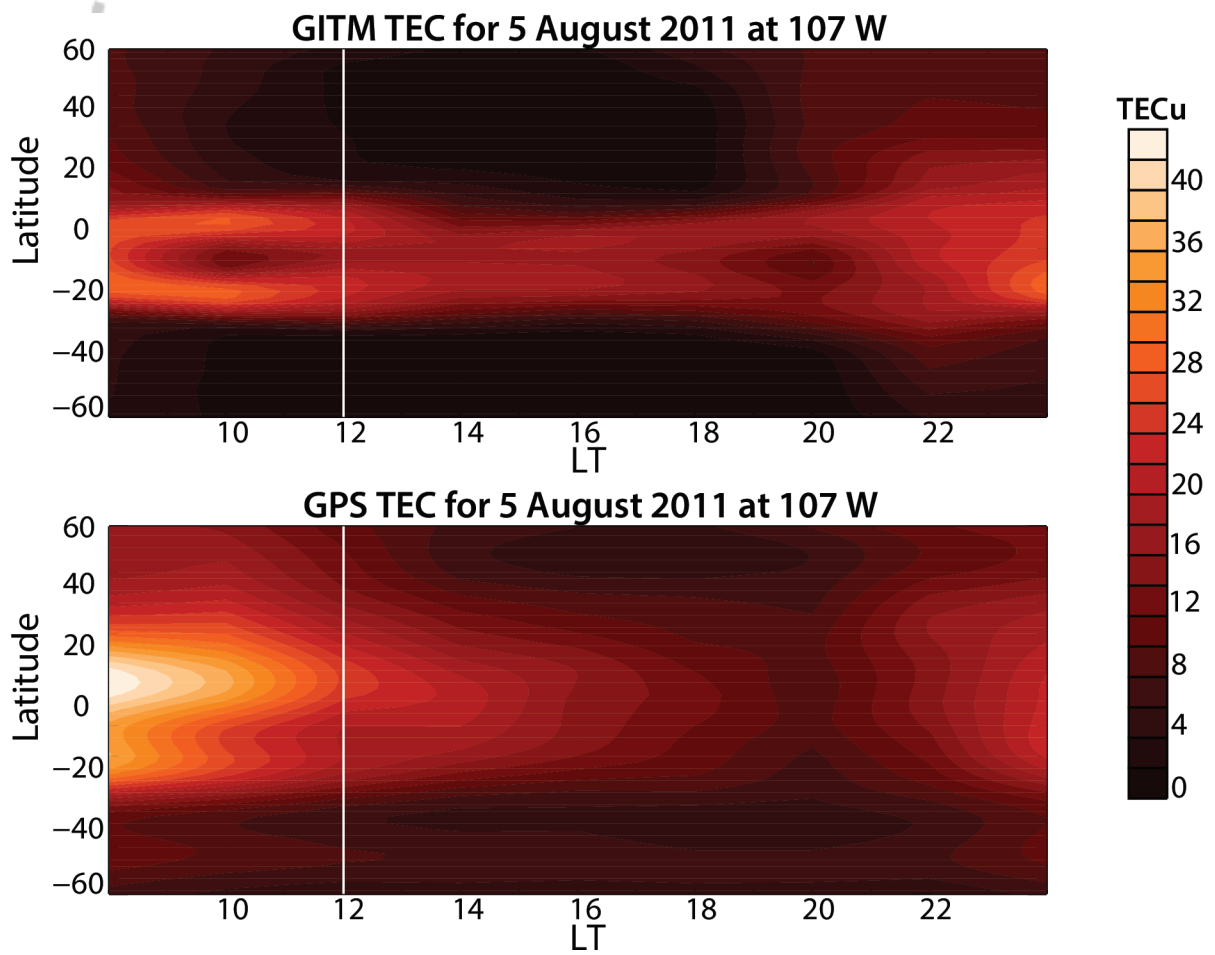
**Figure 6.** Percent Change between quiet and storm time  $[O]/[N_2]$  ratio for selected experimental storm onset times. Each panel is for a constant longitude and the colors indicate the percent change in latitude and local time.

**Figure 7.** Wind vectors for the experimental storm onset times. Each panel is for a constant longitude, the contoured colors behind the vectors indicate the zonal wind change in latitude and local time. The longitude depicted corresponds to the longitude of 1200 LT at the time of the onset of storm conditions.

**Figure 8.** August 2011 International Geomagnetic Reference Field (IGRF) intensity [ $10 \cdot nT$ ] are plotted as solid black contours. The ion vertical velocity [m/s] at 1600 LT for the modeling experiments shown in Figure 7 are shown for quiet conditions, the August 2011 geomagnetic storm conditions and the difference between these conditions (storm - quiet).

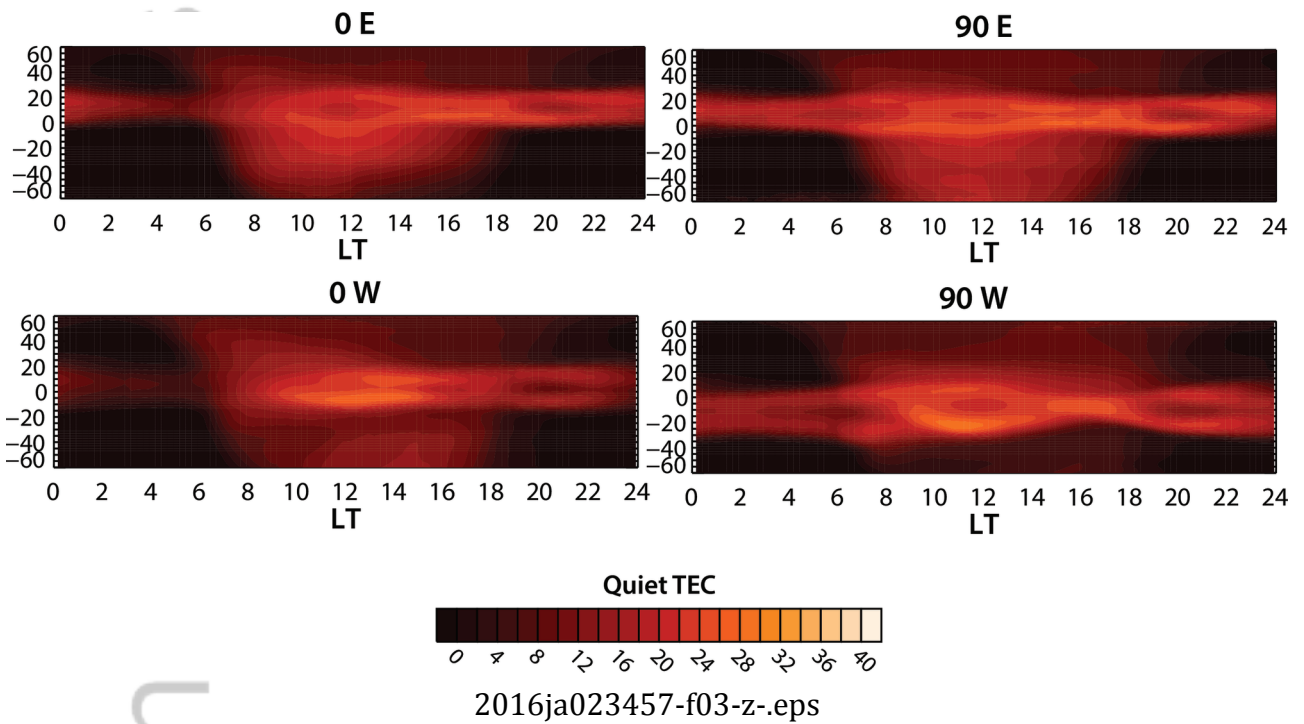


2016ja023457-f01-z-.eps

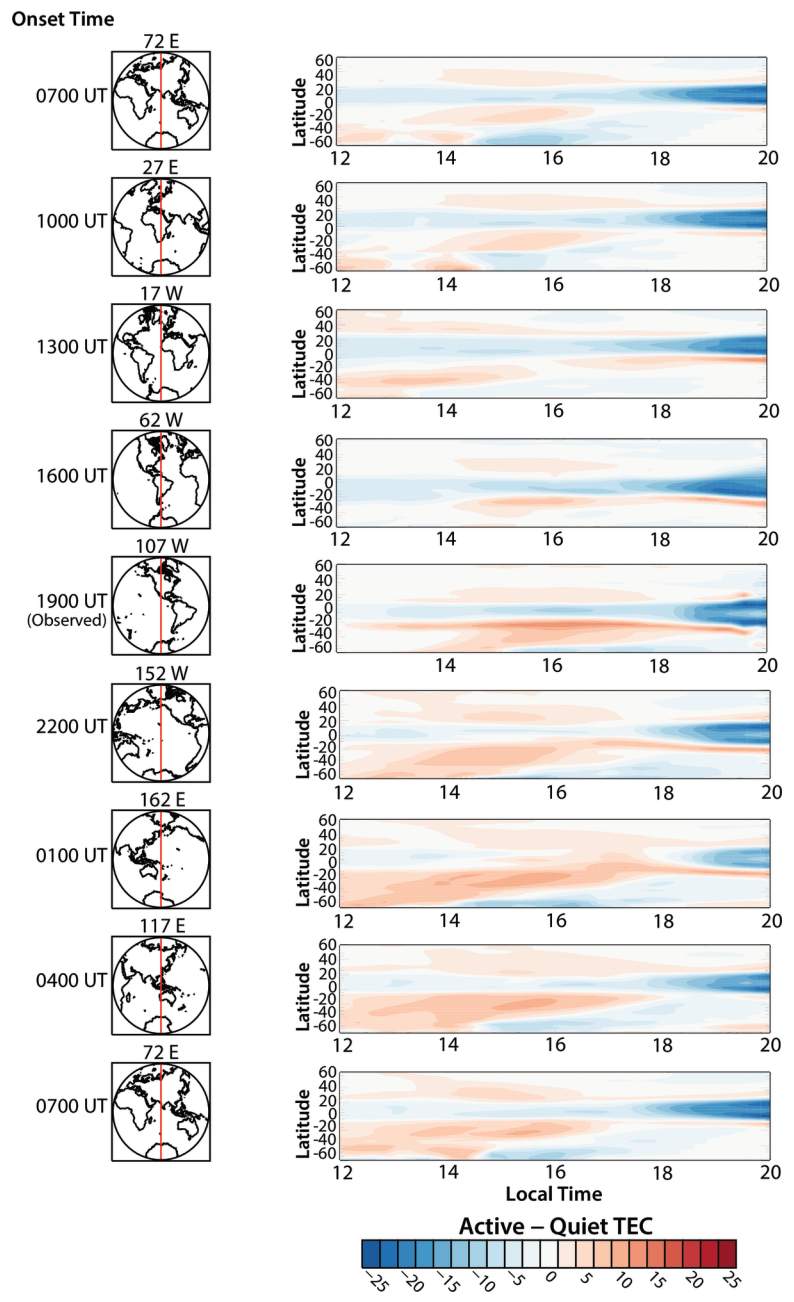


2016ja023457-f02-z-.eps

cript

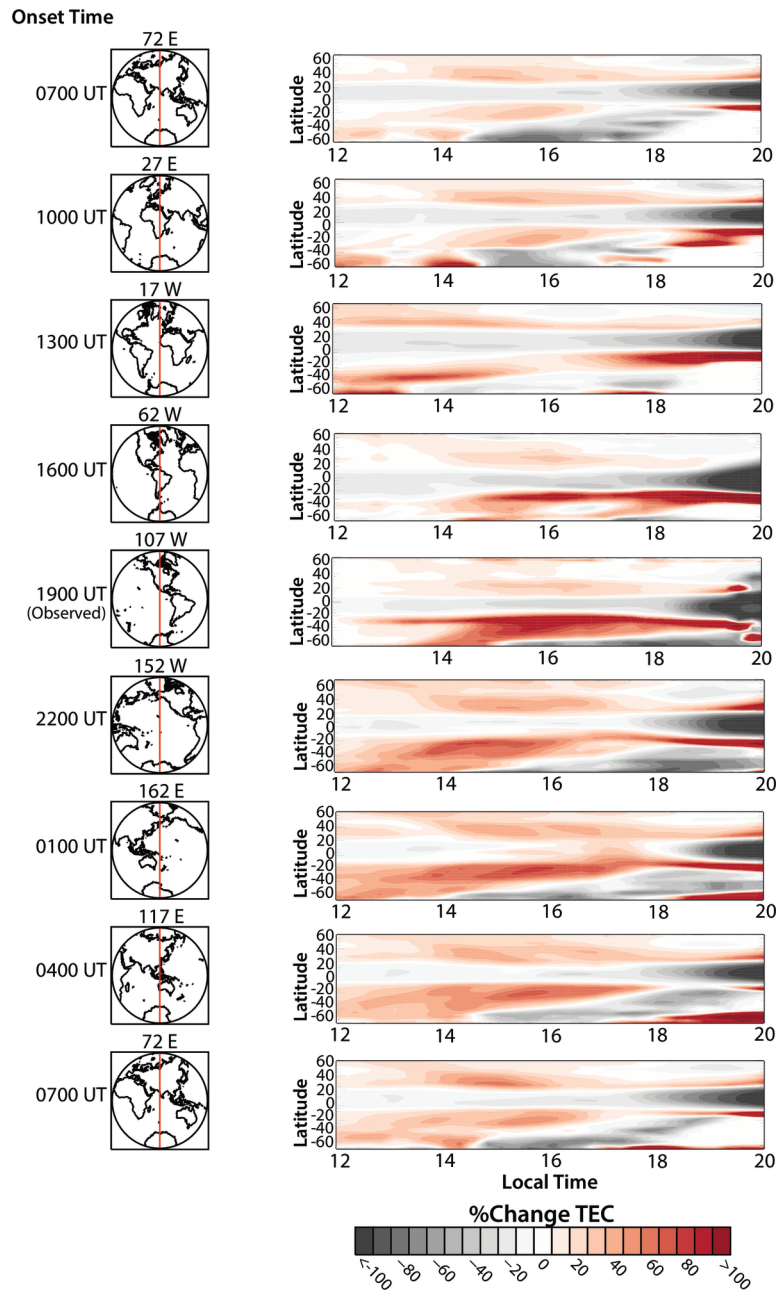


Auth



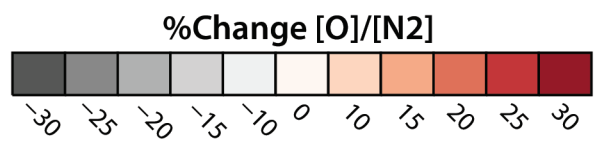
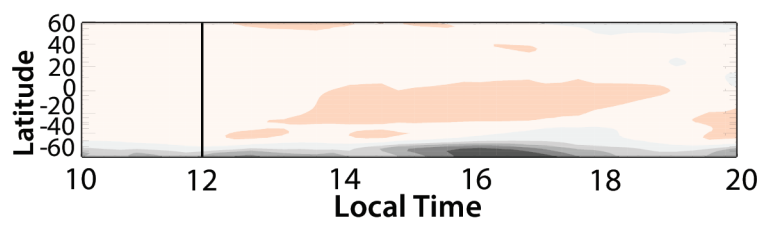
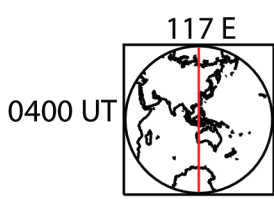
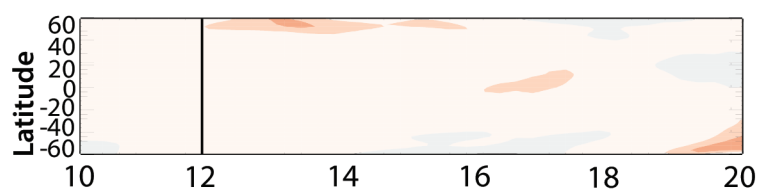
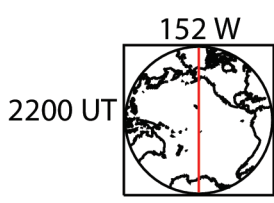
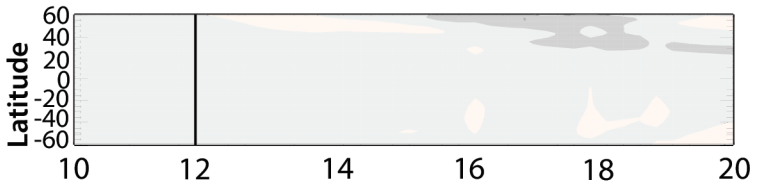
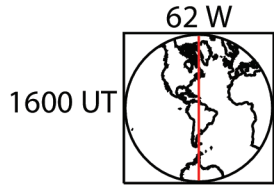
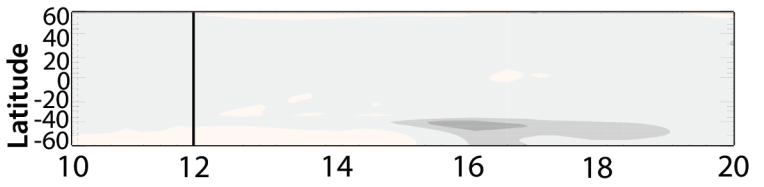
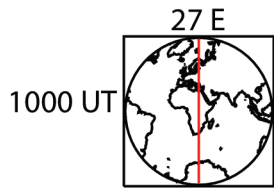
2016ja023457-f04-z-eps





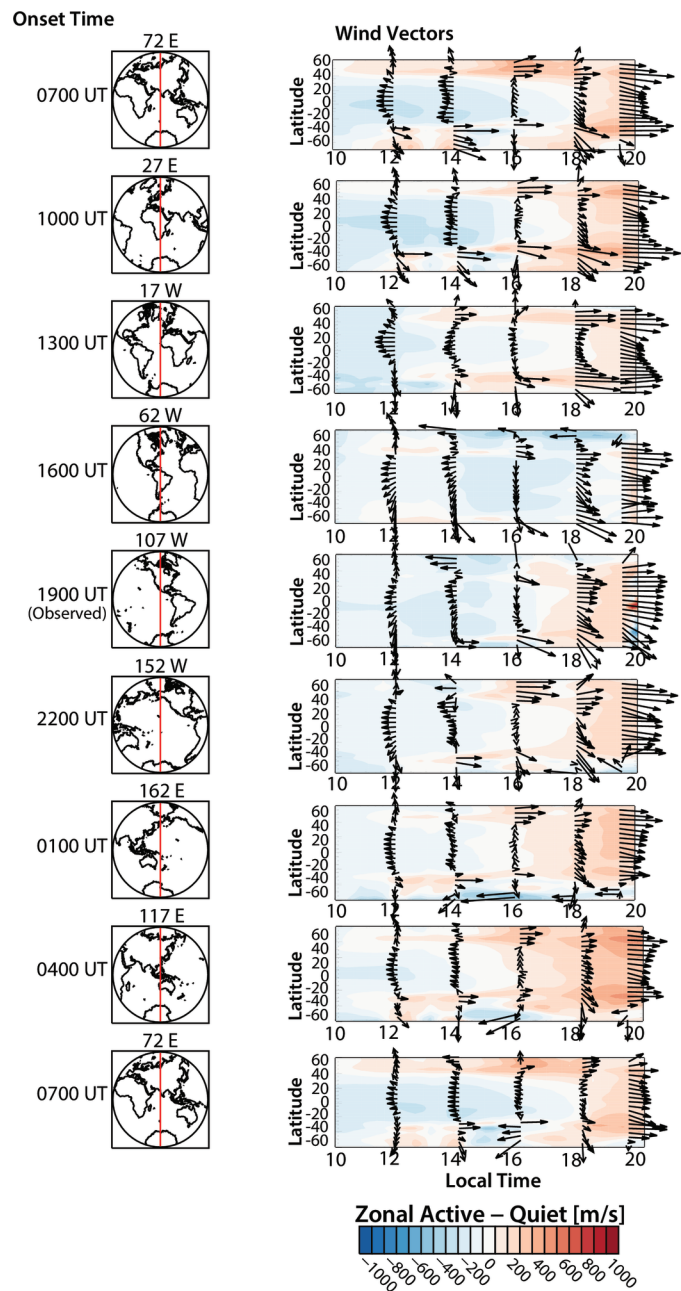
2016ja023457-f05-z-.eps

pt  
Onset Time

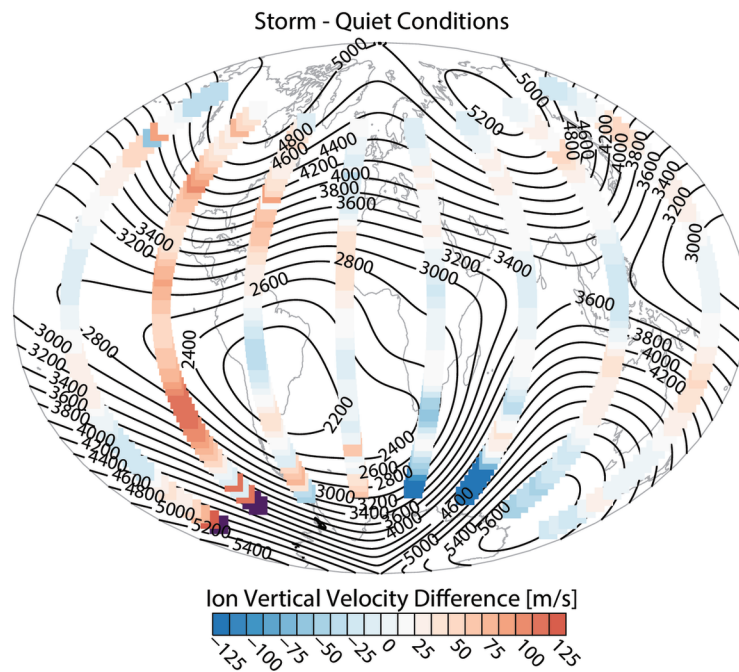
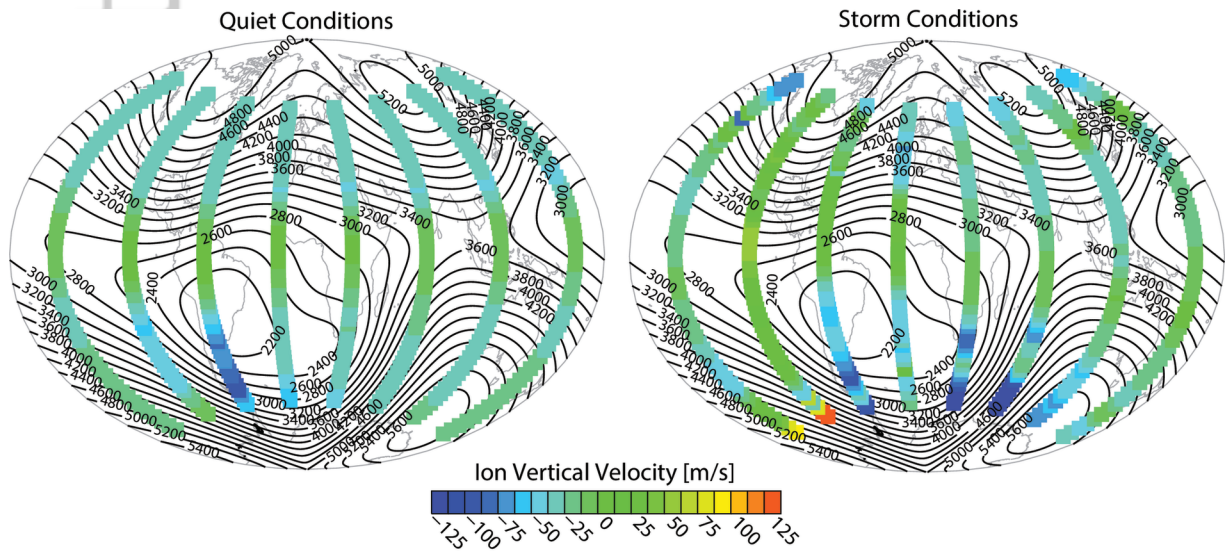


2016ja023457-f06-z-eps

AI



2016ja023457-f07-z-.eps



2016ja023457-f08-z-.eps